THE JOURNAL OF COMPARATIVE NEUROLOGY 365:141–158 (1996)

Activity-Related Features of Synapse Morphology: A Study of Endbulbs of Held

DAVID K. RYUGO, MELISSA M. WU, AND TAN PONGSTAPORN
Center for Hearing Sciences, Departments of Otolaryngology–Head and Neck Surgery (D.K.R., M.M.W., T.P.) and Neuroscience (D.K.R.), Johns Hopkins University School of Medicine, Baltimore, Maryland 21205

ABSTRACT

The myelinated fibers of the auditory nerve can be divided into two separate populations on the basis of sensitivity to sound, average levels of spike activity, and central branching patterns. The synaptic endings of these populations were investigated for the presence of structural specializations that might correlate with levels of neural activity. We applied intracellular recording and staining methods in cats to analyze directly the relationship between spike activity and the structure of synapses using endbulbs of Held, the large synaptic endings in the anteroventral cochlear nucleus. Endbulbs from fibers having low or high levels of activity were examined and compared using light and electron microscopic methods. All endbulbs exhibited relatively large but incomplete coverage by one-to-several lamellae of glial processes. Endbulbs of high activity fibers were large and contained larger mitochondria than endbulbs of low activity fibers. Furthermore, the synapses of high activity endbulbs were on average smaller but more numerous, possessed greater numbers of associated synaptic vesicles, and exhibited greater curvature of their postsynaptic densities. These structural features are hypothesized to reflect specializations that optimize synaptic transmission.

Indexing terms: active zones, electron microscopy, hearing, spontaneous discharge rate, synaptic vesicles

The importance of neural activity on the normal development and function of synapses has received strong experimental support (e.g., Shatz and Stryker, 1978; Shatz, 1990; Goodman and Shatz, 1993). Manipulations that deprive sensory systems of input produce striking atrophic effects (Powell and Erulkar, 1962; Van der Loos and Woolsey, 1973; LeVay et al., 1980; Born and Rubel, 1985; Shatz and Stryker, 1988; Kaas, 1991), whereas selective activation can produce somatic enlargement (Wiesel and Hubel, 1963; Benson et al., 1984; Moore, 1985), terminal swelling (Heuser and Reese, 1973; Boyne et al., 1975; Burwen and Satir, 1977), dendritic spine alterations (Fifková and van Harreveld, 1977; Fifková and Morales, 1992), and modifications in receptive field properties (Gilbert and Weisel, 1990; Diamond et al., 1993; Weinberger, 1995). These kinds of activity-related changes in the central nervous system represent the basis for ideas that postsynaptic structure and function depends on the type and level of presynaptic activity.

In the auditory system, much progress has been made along the lines of examining central effects of sensory deprivation. Changes in the central nervous system have been produced through destruction of the sensory receptors (Parks, 1979; Trune, 1982; Born et al., 1991) or pharmacologic blockade of electrical activity in the auditory nerve (Sie and Rubel, 1992; Pasik et al., 1994). The severity of neural alterations depends on the species and the age of the animal at the time of manipulation (e.g., Powell and Erulkar, 1962; Born and Rubel, 1985; Hashisaki and Rubel, 1989) and on the method of sensory deprivation (Tucci et al., 1987). Furthermore, destruction of the sensory cells produces deafness but can simultaneously damage the innervating primary fibers, so that central alterations can result from direct or indirect neural insult rather than from simply a loss of activity per se (Leake and Hradek, 1988; Gil-Loyzaga and Pujol, 1990). The nature of central change may not necessarily reflect only a diminution of activity but may also be confounded by experimentally induced degeneration and a corresponding reorganization and expansion of intact neighboring regions (Nordeen et al., 1983; Moore and Kowalchuk, 1988; Schwaber et al., 1993). Regardless, it seems safe to conclude that acoustic deprivation induces pathologic changes in the central auditory pathway.

There have been other studies that selectively affect particular regions of the auditory system. These studies

Accepted August 11, 1995.

Address reprint requests to David K. Ryugo, Center for Hearing Sciences, Johns Hopkins University School of Medicine, 510 Traylor Research Building, 720 Rutland Ave., Baltimore, MD 21205. E-mail: dryugo@bme.jhu.edu

utilized frequency-specific training (Bakin and Weinberger, 1990; Recanzone et al., 1993) or selective cochlear lesions (Robertson and Irvine, 1989) and argued for stimulus-specific plasticity. How individual neurons contribute to the response plasticity of the population, however, was not resolved. Why some sites exhibit plastic changes and some do not (Weinberger et al., 1993) is another issue that merits further examination. In view of these kinds of complex issues, we have considered a simpler model of activity-related synaptic features using the normal auditory system of mature cats. Our goal was to establish a baseline of synaptic morphology as it related to synaptic activity.

The auditory nerve is an excellent model with which to study activity-related features of synaptic structure. Our focus is on the myelinated fiber population whose peripheral processes terminate as radial fibers against the base of inner hair cells (Spoendlin, 1978; Kiang et al., 1982). These fibers convey acoustic information into the brain, and individual fibers can be described by two fundamental properties: frequency selectivity and spontaneous discharge rate. Frequency selectivity is represented by that tonal frequency to which the fiber is most sensitive, referred to as the characteristic frequency (CF). CF reflects the longitudinal position along the cochlea where the peripheral process terminates (Liberman, 1982b). Spontaneous discharge rate (SR) is that spike activity (in spikes per second; s/s) that occurs in the absence of experimentally controlled acoustic stimulation (Kiang et al., 1965; Liberman, 1978). SR can range from near zero to greater than 100 s/s; and across the audible frequency range, there is a bimodal distribution of SR in the population of auditory nerve fibers: one group has an SR that is less than 5 s/s and the other has an SR that is greater than 20 s/s (Kiang et al., 1965; Evans and Palmer, 1980). Thus, it is possible to compare the anatomy and physiology of fibers from each SR group while keeping CF constant.

In the present study, we used intracellular recording and staining methods to label individual auditory nerve fibers after first characterizing some of their physiologic properties. Because the two populations differ in their spontaneous activity and in their thresholds for evoked activity, low SR fibers are expected to exhibit much less overall spike activity than high SR fibers. We examined the morphologic features of labeled synaptic endings, specifically, the large, axosomatic endbulbs of Held, by using light and electron microscopy. In this way, we directly determined the structure of synapses of fibers having high versus low activity levels and analyzed the relationship between neural activity and synaptic morphology.

METHODS

Animal preparation

Two male cats, each weighing 2.5 kg and having clean external and middle ears, were used for the present study. Each cat was anesthetized with an intraperitoneal injection (0.4 cc/kg body weight) of diallyl barbituric acid (100 mg/ml) in urethane solution (400 mg/ml). Supplemental doses were administered when necessary to keep the animal areflexic. Body temperature was monitored with a rectal thermometer and maintained at 37°C using a heating pad and a heated sound-proofed chamber.

The trachea was cannulated, an indwelling catheter was inserted into the cephalic vein for administration of balanced salt solutions, and the skin and muscle layers overlying the skull were removed. Each bulla was opened to allow for round window recordings, and the external meati were cut near the tympanic ring to insert hollow ear bars for delivering calibrated acoustic stimuli (Sokolich, 1977). The posterior fossa was opened using rongeurs, the dura reflected over the cerebellum, and the cerebellum retracted to expose the auditory nerve as it extended from the internal auditory meatus to the cochlear nucleus. N1 potentials to 100-μs 4V peak-to-peak clicks were just detectable at approximately 0–5 dB SPL, indicating that the cats had normal hearing.

Single unit recordings

Recording micropipettes were placed into the nerve under direct visual control using an operating microscope. For each unit, a threshold tuning curve and a 10-second period of spontaneous activity were obtained before and after injection of horseradish peroxidase (HRP). The similarity of pre- and postinjection response properties and a continuously negative DC potential provided evidence that the injected fiber was the same one from which recordings were obtained. An automated tuning curve maker (Liberman, 1982b) was used to determine fiber CF. For the present study, fibers of low SR were injected on one side and fibers of high SR were injected on the opposite side. In this way, labeled fibers could not be confused with respect to SR grouping.

Staining and tissue preparation

Individual fibers were marked by iontophoresing a 10% HRP solution in 0.05 M Tris buffer (pH 7.3) containing 0.15 M KCl through micropipettes having impedances of 24–34 MΩ. Approximately 24 hours after the last fiber was injected, the cat was given a lethal dose of Nembutal, artificially respired, and perfused through the heart with 100 cc isotonic saline (25°C) with 0.1% $NaNO_2$ in 0.12 M cacodylate buffer (pH 7.4), followed immediately by 0.5 liter of fixative containing 0.5% paraformaldehyde, 1% glutaraldehyde, and 0.008% $CaCl_2$ in 0.12 M cacodylate buffer (pH 7.4), and then by 1.5 liters of a second fixative containing 1.25% paraformaldehyde, 3% glutaraldehyde, and 0.008% $CaCl_2$ in the same buffer solution. Following perfusion, the brain was dissected from the skull, and then the brainstem was isolated and stored overnight in the first fixative. The next morning, each cochlear nucleus was oriented and embedded in a gelatin–albumin mixture hardened with glutaraldehyde so that 50-μm-thick Vibratome sections could be collected approximately parallel to the lateral surface of the nucleus. Sections were kept in serial order, rinsed several times in 0.1 M Tris buffer (pH 7.5), and incubated for 1 hour in 0.5% $CoCl_2$ in Tris buffer. Sections were then rinsed in Tris buffer, rinsed again in 0.1 M phosphate buffer (pH 7.3), and incubated for 1 hour with 0.05% 3,3′-diaminobenzidine (DAB; Sigma, grade II Tetra HCl) in phosphate buffer. The tissue was reacted for an additional hour with a fresh solution of DAB containing 0.01% H_2O_2. Sections were then placed in 1% OsO_4 for 15 minutes, rinsed 6 × 5 minutes in 0.1 M maleate buffer, pH 5.0, stained en bloc for 1 hour in 2% uranyl acetate, rinsed again in maleate buffer, dehydrated in a series of graded alcohol concentrations, and infiltrated with Epon. Sections were embedded in fresh Epon between two sheets of Aclar (Ted Pella, Inc.).

Once the Epon had hardened, sections were taped to microscope slides and examined with the aid of a light

TABLE 1. Physiologic Properties and Light Microscopic Morphometry

	Endbulb	CF (kHz)	SR (s/s)[1]	Form factor	EB area (μm^2)	SBC area (μm^2)	Estimated synapses/endbulb
Cat 20							
Left auditory nerve							
	Lo1 (10)	1.0	0.01	0.42	386.0	633.6	237
	Lo2 (11)	0.6	0.07	0.35	246.5	705.8	520
	Lo3 (8d)	1.4	0.27	0.45	284.4	760.7	499
	Lo4 (7)	1.0	0.40	0.49	298.9	817.4	508
Right auditory nerve							
	Hi1 (5d)	1.8	62.0	0.62	450.4	713.7	1,730
	Hi2 (1b)	1.1	56.0	0.82	750.4	1,061.0	1,972
	Hi3 (4c)	0.5	60.4	0.76	415.7	840.9	2,022
Cat 32							
Left auditory nerve							
	Hi4 (13b)	2.6	76.0	0.57	379.6	605.5	1,159
Right auditory nerve							
	Lo5 (9a)	1.8	0.0	0.37	224.8	427.9	274
Means							
Low SR fibers				0.41 ± .06	288.1 ± 62.1	669.1 ± 150	407 ± 139
High SR fibers				0.69 ± .12	499.0 ± 170	805.3 ± 195	1,720 ± 395
Mann-Whitney U test				$P < 0.02$	$P < 0.03$	$P = 0.3$	$P < 0.01$

[1]Spikes per second.

microscope. Sections were drawn at a total magnification of 25× with the aid of a light microscope and drawing tube, and relevant labeled structures were redrawn at a total magnification of ×2,500 (×100 oil immersion lens, NA 1.25). Terminal endbulbs were dissected with the aid of an operating microscope and re-embedded into BEEM capsules. Serial ultrathin sections were collected on Formvar-coated slotted grids, stained with 7% uranyl acetate, and viewed with a JEOL 100CX electron microscope.

Data analysis

We analyzed a total of nine darkly labeled fibers from these two cats: five low SR fibers and four high SR fibers (Table 1). Each labeled fiber was first reconstructed through serial 50-μm-thick sections at a total magnification of ×325 with the aid of a light microscope and drawing tube to determine the spatial position of its trajectory through the nucleus and to map the location of its bifurcation in the auditory nerve root. The location of the endbulb and bifurcation for each fiber was normalized by determining its dorsoventral trajectory within the nucleus and comparing it with the total dorsal-to-ventral range of the nucleus. The normalized position of these structures was compared with the tonotopic map of the nucleus (Bourk et al., 1981; Ryugo and May, 1993) and used as independent verification of the CF determinations made at the time of the intracellular injection.

Each endbulb and its postsynaptic spherical bushy cell were then drawn at a total magnification of ×2,500, and the drawings were further enlarged to a final magnification of ×5,600. From these enlargements, endbulb, cell body, and nuclear silhouette areas and perimeters were determined by computerized planimetry (SigmaScan, Jandel Scientific). For the endbulbs, the ratio of the silhouette area divided by the perimeter (units dropped) yielded a value referred to as the "form factor," where values below 0.52 corresponded to low SR endbulbs and values above 0.52 corresponded to high SR endbulbs (Sento and Ryugo, 1989).

Endbulbs were then examined through an electron microscope. Because each section is relatively thin compared with the endbulb, any particular section contained only pieces of the labeled ending, and individual pieces are referred to as "ending profiles." The size, shape, and frequency of synapses were determined by reconstructing individual postsynaptic densities (PSDs) through serial sections and then rotating the stack of sections using a computerized three-dimensional imaging system (Eutectics Electronics). Synapses were reconstructed from multiple regions of the endbulb for which we had an unbroken series of at least 20 ultrathin sections. Ultrathin section thickness was estimated using standard interference reflection colors as the sections floated in the knife trough. Our sections were silver in color, more gray than gold, and we estimated their thickness as 75 nm. This value is consistent with our serial reconstructions because 13 sections, when rotated 90° and viewed en face, spanned slightly less than 1 μm as determined by our calibration grid, and 14 sections slightly exceeded 1 μm.

Other analyses were conducted from these same sections, but in such instances 10–20 sections were selected for having somewhat uniform spacing as they spanned the endbulb. Every labeled profile from each selected section was photographed and analyzed. Each labeled profile with its associated mitochondria, PSDs, and apposition length (Fig. 1) was traced from electron micrographs (total magnification of ×69,000) and then measured by computerized planimetry. Apposition length was defined as the membrane abutment between pre- and postsynaptic structures. Postsynaptic densities appeared as thickenings in the postsynaptic membrane opposite the synaptic cleft and morphologically represented the synapse. The degree of curvature of each PSD was calculated using the formula $1/r = 8a/(4a^2 + b^2)$, where r is the radius of curvature of a circle passing through the points at the ends of the PSD, b is the chord length passing through the opposite ends of the PSD, and a is the perpendicular height of the arch at the midpoint of b (Cooke et al., 1974). Mitochondrial area was measured, and the volume fraction was calculated as a proportion of the terminal profile area. We analyzed the diameter of synaptic vesicles, the number of synaptic vesicles per profile and per PSD per profile using electron micrographs at a total magnification of ×138,000.

All measurements are accompanied by means and standard deviations. Statistical comparisons were made using two-tailed, unpaired, Student's t test, Mann-Whitney U tests, and analysis of variance (ANOVA). Both parametric and nonparametric tests were used because the data were not always normally distributed, and ANOVA was used to control for interactions within the variables. All statistical

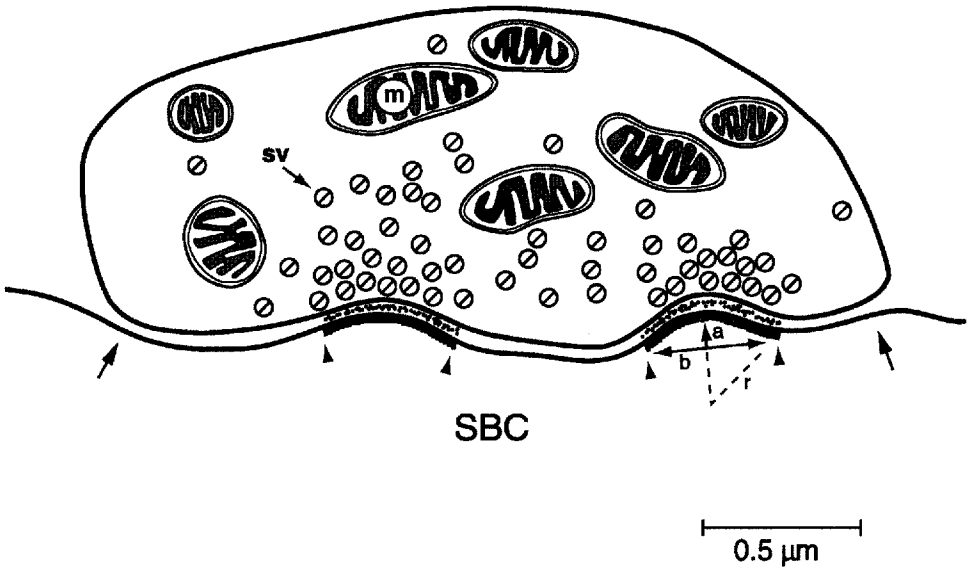

Fig. 1. Schematic diagram of a terminal ending illustrates the morphologic features that were analyzed with an electron microscope. For each ending profile, synaptic vesicles (sv), mitochondria (m), and postsynaptic densities (PSDs) were counted. The length of the PSD (flanked by arrowheads) was measured. Synaptic vesicle diameters are indicated by straight lines in the diagram and are all parallel to each other; the orientation of the diameters was selected at random. Mitochondria size is represented by silhouette area. The apposition of the ending (between the arrows) with the postsynaptic target was measured. The radius of PSD curvature (r) was calculated using the chord length (b) and the line drawn from the peak of the curve perpendicular to this chord (a) in the formula $1/r = 8a/(4a^2 + b^2)$. SBC, spherical bushy cell.

tests were consistent at the 95% confidence level, but the Mann-Whitney U test proved most conservative so its P values are presented. We ran statistical tests using the number of endbulbs (not the number of cats) when calculating P values. Although we recognize that statistical significance is not necessarily equivalent to biological significance, the raw data indicate clear differences between the two SR groups.

RESULTS

The present results are based on light and electron microscopic analyses of nine terminal endbulbs of Held, each from labeled auditory nerve fibers that were intracellularly injected with HRP after first being physiologically characterized through the same micropipette. Five low SR auditory nerve fibers and four high SR fibers were histologically recovered from two cats (Table 1). Each nerve contained a restricted number of fibers belonging to only one SR group. Additional criteria and considerations were used to identify more precisely the labeled fibers in each nerve. The injection site is marked by a distinct swelling along the axon, and we derived fiber identity by correlating the position of the micropipette tip at the time of injection with the location of the fiber swelling found in the tissue (Fekete et al., 1984). The trajectory of auditory nerve fibers and the location of their terminal endbulbs in the cochlear nucleus were also systematically correlated to their CFs (e.g., Ryugo, 1992; Ryugo and May, 1993), and so we used position along the dorsoventral axis within the anteroventral cochlear nucleus (AVCN) as an independent verification of fiber identity. Thus, we could relate unit physiology to fiber morphology with a high degree of confidence.

Auditory nerve fibers

Fibers from each cat were similar in their frequency response characteristics but distinctly different in their average spike activity as indicated by SR. This strategy permitted us to analyze synaptic endings and their postsynaptic targets in separate cochlear nuclei, but within the same cat, thereby reducing interanimal variability. The general morphologic features of the labeled fibers were consistent with previous descriptions (e.g., Fekete et al., 1984; Ryugo and May, 1993). That is, after the bifurcation, the ascending branch projected in a relatively straight trajectory through the AVCN and gave rise to 5–11 primary collaterals. Each collateral branched several more times and, for the most part, terminated within several hundred micrometers from the parent fiber; collaterals of low SR fibers branched much more profusely than did those of high SR fibers. Distinct swellings marked the tips of the collaterals. In addition, each low SR fiber gave rise to 1–3 long, highly ramified collateral arborizations that distributed en passant and terminal swellings just beneath the superficial layer of granule cells along the lateral edge of the AVCN and dorsally within the small cell cap. As the ascending branch approached the rostral limits of the nucleus, it turned back sharply and blossomed into the endbulb of Held (Lorente de Nó, 1981; Ryugo and Fekete, 1982; Sento and Ryugo, 1989).

Endbulbs

Each fiber was darkly labeled and gave rise to a well-defined terminal endbulb. Individual endbulbs were located in the anterior part of the anterior division of the AVCN (Fig. 2). The position of each endbulb was reconstructed through serial sections of the cochlear nucleus and was found to be consistent with the tonotopic axis of the nucleus (Bourk et al., 1981; Ryugo and May, 1993). There was no apparent relationship between CF, SR, and the rostral-caudal position of the endbulb.

Endbulbs of Held are typified by the emergence of several thick, gnarly branches that divide repeatedly to form a

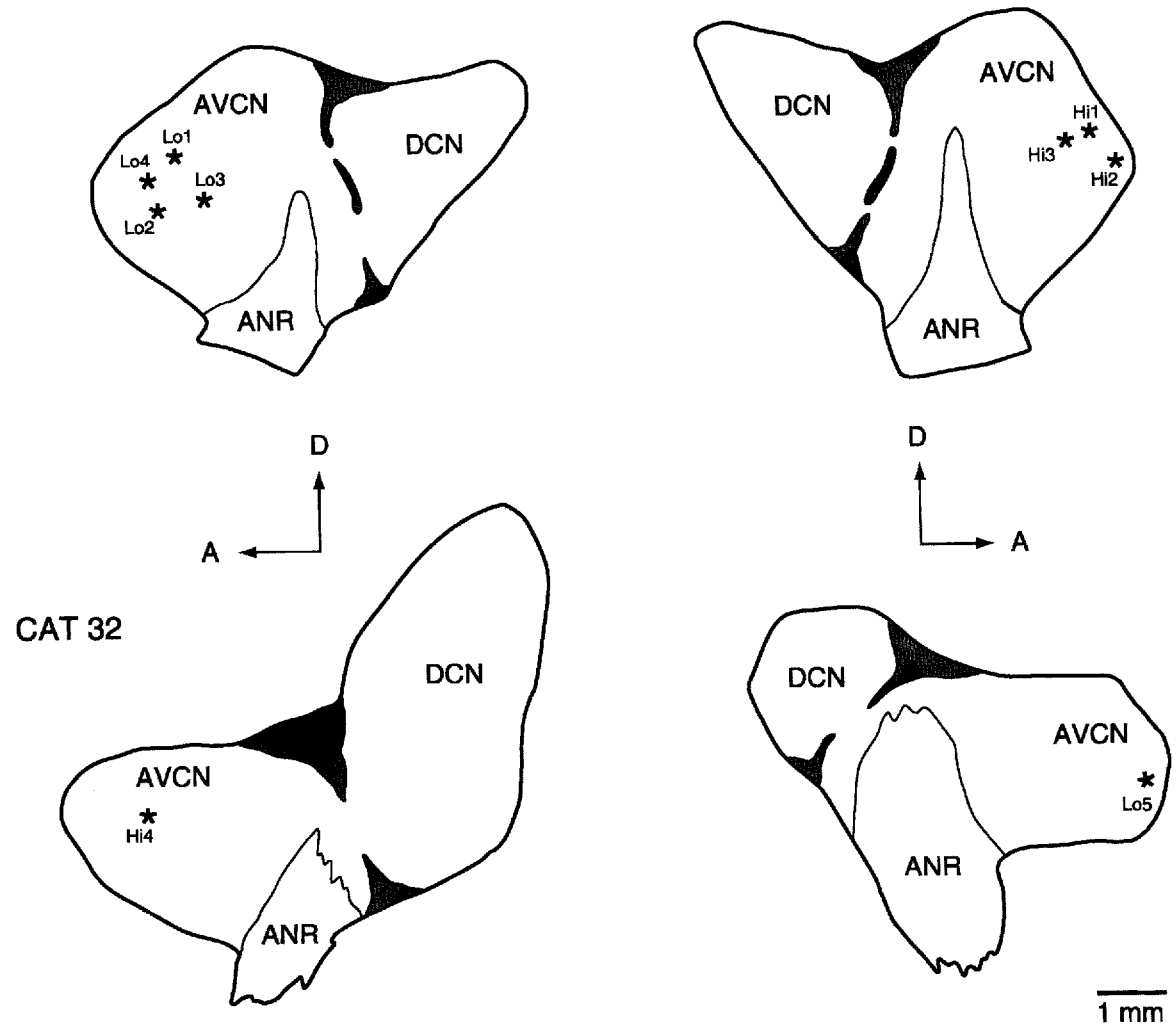

Fig. 2. Locations of endbulbs (asterisks) in the cochlear nucleus. Each location is mapped onto a drawing tube reconstruction of the nearest histologic sections in a plane parallel to the lateral surface of the nucleus. **Top:** Location of endbulbs from the cochlear nuclei of Cat 20. In the left AVCN, the loci of four low (Lo1–4) spontaneous discharge rate (SR) endbulbs (characteristic frequencies [CFs], 0.6–1.4 kHz; SR, 0.01–0.4 s/s) are shown. In the right AVCN, the loci of three high (Hi1–3) SR endbulbs (CFs, 0.5–1.8 kHz; SR, 56–62 s/s) are illustrated. Endbulb features are provided in Table 1. **Bottom:** Locations of endbulbs from the cochlear nuclei of Cat 32. High SR endbulb in the left AVCN (CF, 2.6 kHz; SR, 76 s/s) and low SR endbulb in the right AVCN (CF, 1.8 kHz; SR, 0 s/s). Anterior (A) and dorsal (D) directions are indicated. AVCN, anteroventral cochlear nucleus; DCN, dorsal cochlear nucleus; ANR, auditory nerve root. Stipple indicates granule cell domains.

clawlike arborization, which in turn clasps approximately one-half of a single cell body (Figs. 3, 4). The endbulb arborization is marked by multiple swellings of various sizes and shapes. Short filopodial collaterals may extend away from the arborization and often terminate with a swelling; these collaterals are more frequently associated with endbulbs of low SR fibers. The collaterals that project from the main body of the endbulb can associate with short segments of the primary dendritic stalks of the postsynaptic neurons or travel some distance (up to several hundred micrometers) to terminate on unknown structures. The endbulbs from high SR fibers exhibit thicker branches and larger, but fewer, swellings and lobules when compared with those of low SR fibers. This appearance is quantifiable by determining silhouette area and silhouette perimeter and by forming the form factor ratio. Endbulbs of high SR fibers had an average form factor value of 0.69 ± 0.12, whereas that of low SR fibers had a value of 0.41 ± 0.06 ($P < 0.02$). Form factor values of the present study are consistent with previous published results (Sento and Ryugo, 1989). The high SR endbulbs also exhibited larger average silhouette areas (499.0 ± 170 μm^2) than did the low SR endbulbs (288.1 ± 62.1 μm^2, $P < 0.03$).

Spherical bushy cells

Cradled within each labeled endbulb was a spherical bushy cell (criteria of Osen, 1969; Cant and Morest, 1979). At the light microscopic level, these cells exhibited a round-to-oval cell body (roughly 30 μm in diameter) and a centrally placed, round nucleus capped with Nissl sub-

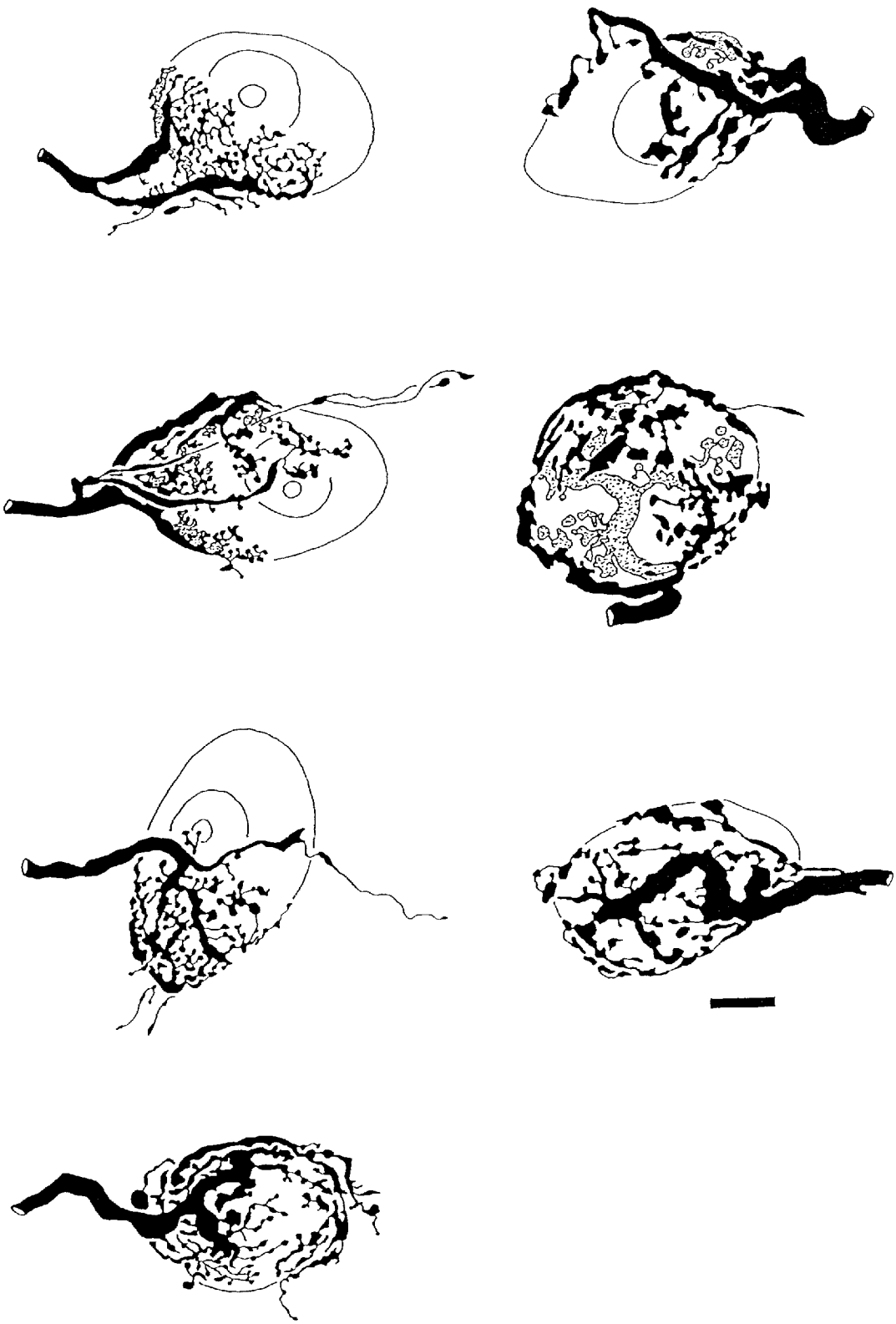

Fig. 3. Drawing tube reconstructions of the seven endbulbs analyzed from Cat 20. Endbulbs are from low SR fibers (**left**) and high SR fibers (**right**). They are presented in the same order, from top to bottom, in which they are listed in Table 1. Endbulbs of low SR fibers have thinner branches and smaller varicosities and swellings than those of high SR fibers. Stippling indicates parts of the endbulb on the far side of the enclosed cell body, and the cell body is outlined. The difference in endbulb appearance of the separate SR fibers is quantifiable by the ratio of the endbulb silhouette area divided by endbulb perimeter. Scale bar = 10 μm.

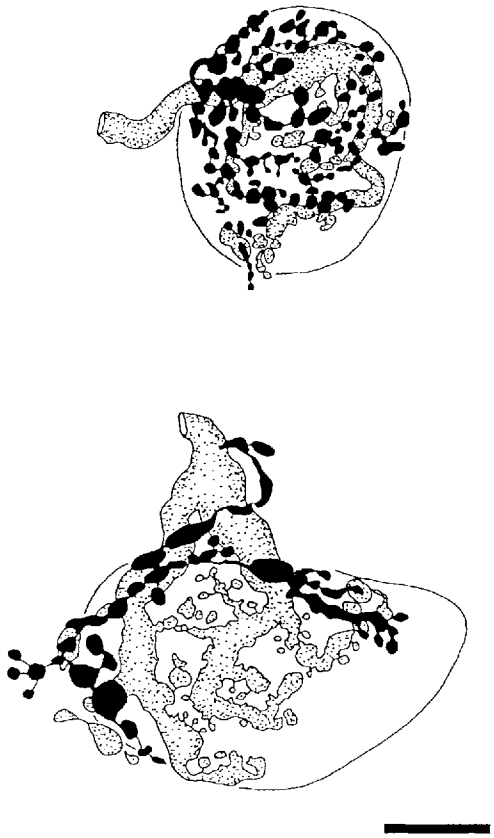

Fig. 4. Drawing tube reconstructions of two endbulbs analyzed from Cat 32. Endbulb from low SR fiber (**top**) and high SR endbulb (**bottom**) are illustrated. Stippling indicates parts of the endbulb on the opposite side of the cell body, and the cell body is outlined. The endbulb from the low SR fiber exhibits light microscopic features typical of the group in exhibiting thinner branches and more but smaller varicosities and swellings. Scale bar = 10 μm.

stance. One or two primary dendrites could be seen emerging from the cell body when using differential interference contrast microscopy. Cells receiving high SR endbulbs had mean silhouette areas of 805.3 ± 195 μm^2, whereas those receiving low SR endbulbs had mean areas of 669.1 ± 150 μm^2 ($P = 0.3$).

At the ultrastructural level, these cells contained multiple stacks of rough endoplasmic reticulum (ER) plus the usual complement of mitochondria, lysosomes, multivesicular bodies, and an extensive Golgi apparatus. Each cell gave rise to 2–4 primary dendrites. The nucleus was round and pale and contained a single nucleolus. There was a prominent accumulation of rough ER on one side of the nucleus that corresponded to the Nissl cap as seen in the light microscope (Fig. 5). Other than a slight size difference, the spherical bushy cells receiving endbulbs from the separate SR fiber groups were morphologically indistinguishable.

Ultrastructural features

Labeled endings are readily distinguishable from unlabeled ones in ultrathin sections (Fig. 5). Because endbulbs were spatially isolated from one another (each was embedded in a separate block), there was no opportunity to confuse the label from one endbulb with that of another despite their similarity in CFs. Profiles of sectioned endbulbs exhibited internal features typical of primary endings; that is, they contained mitochondria and numerous clear, round synaptic vesicles. Synaptic junctions were present that featured punctate, asymmetric postsynaptic densities, an assemblage of vesicles adjacent to the presynaptic membrane, and dense, fuzzy material within the intercellular cleft. The postsynaptic density of the cell body typically bulged out toward the endbulb. These features were analyzed because they are readily observable in normal tissue and they illustrate some of the basic differences between endings of high versus low SR auditory nerve fibers (Figs. 6, 7).

Ending profiles

Profile features. The mean cross-sectional area of labeled profiles was smaller for low SR fibers (1.63 ± 2.2 μm^2, n = 151) than for high SR fibers (2.04 ± 2.7 μm^2, n = 158). In addition, profiles of high SR endings exhibited greater membrane apposition lengths (2.03 ± 1.7 μm) than did profiles of low SR endings (1.72 ± 1.5 μm). These differences ($P < 0.05$) were consistent with light microscopic observations of individual swelling sizes but were only detectable by performing morphometry because of the variability in component shapes and sizes within any single endbulb. The relationship between profile area and apposition length was highly correlated ($r = 0.743$, $P < 0.01$).

Glial processes formed multiple layers and bloblike forms that surrounded or partially surrounded the endbulbs. The layers appeared as thin lamellae that lay in close proximity to the labeled endings and to nonauditory nerve profiles containing flat or pleomorphic synaptic vesicles. We could not determine a relationship between the number of lamellae or the extent of coverage and the SR of the labeled ending.

Mitochondria. These organelles merit attention because they presumably play a key role in the maintenance of metabolic and synaptic activity. There were differences in mitochondrial features when comparing endbulbs of high versus low SR fibers. The silhouette area of mitochondria from high SR endbulbs was larger (0.70 ± 0.04 μm^2, n = 103) than that of low SR endbulbs (0.61 ± 0.03 μm^2, n = 108, $P < 0.03$). Although the average number of mitochondria per profile was similar for high (6.23 ± 6) and low (6.48 ± 7.3) SR fibers, it is inferred that high SR endbulbs contain more mitochondria than low SR endbulbs because they are larger. By taking the average mitochondria fraction from low (18.4 ± 9.2%) and high (15.8 ± 9.0%) SR ending profiles and applying that value to total silhouette area, we estimate that high SR endbulbs contain nearly 50% greater mitochondria volume than low SR endbulbs.

Synaptic vesicles. Synaptic vesicle analysis was conducted on micrographs collected at a magnification of ×56,000 and printed at a total magnification of ×138,000. The mean diameter of synaptic vesicles for endbulbs of high SR fibers was greater when the profile contained a PSD (48 ± 8 nm, n = 764) than when there was no PSD (46 ± 7 nm, n = 380). The mean diameter for vesicles of low SR fibers was greater (48 ± 9 nm, n = 939) when the ending profile contained a PSD than when it did not (44 ± 7 nm, n = 164). There are essentially no differences in synaptic vesicle size when comparing high versus low SR endbulbs, although we measured a small but reliable difference in synaptic vesicle size with respect to proximity of the vesicles to a PSD ($P < 0.03$). These data suggest that synaptic vesicles more distant from the active zone are on average smaller than those nearby.

The number of synaptic vesicles per ending profile and the number per square micrometer were determined. Both

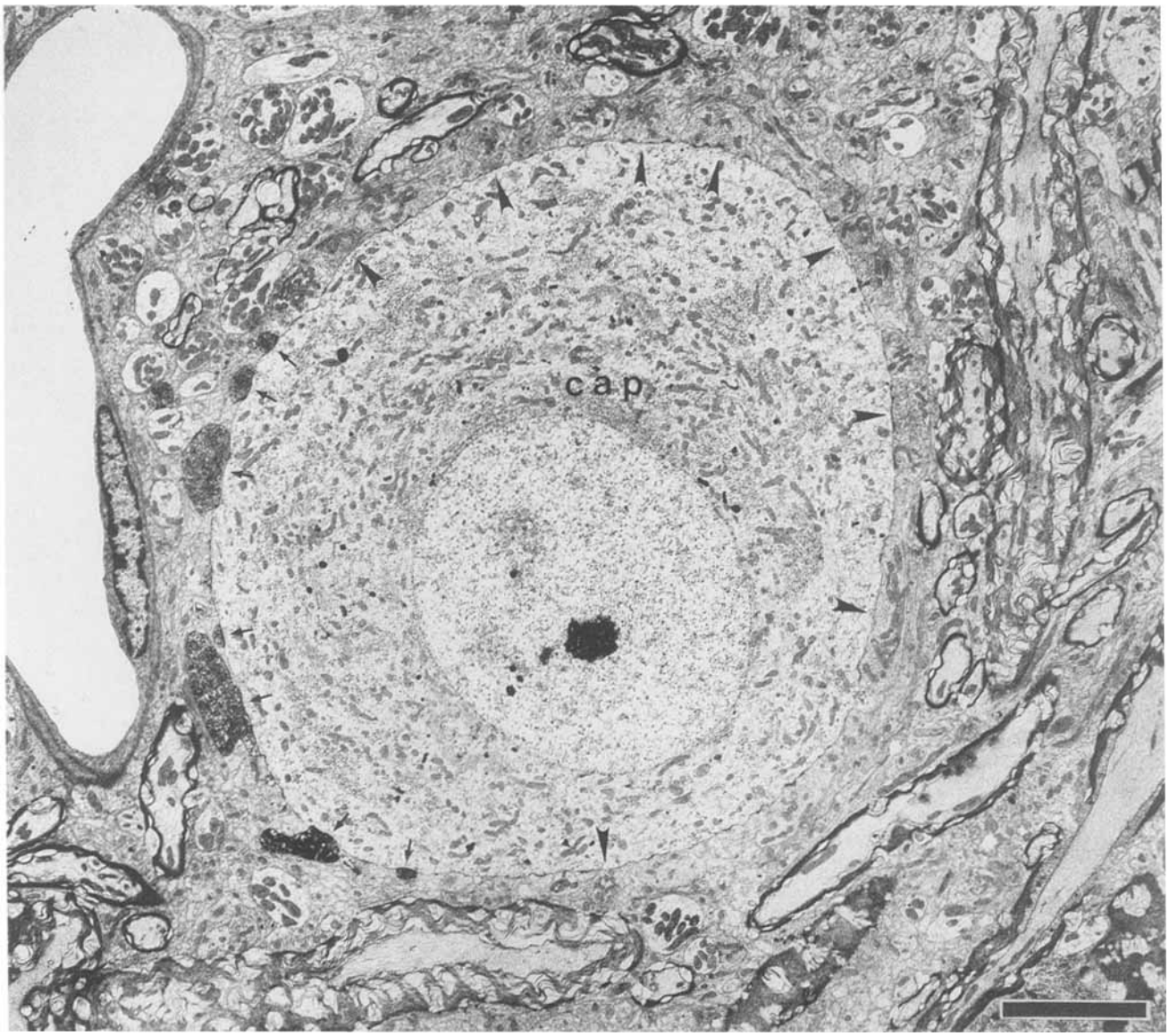

Fig. 5. Electron micrograph through a low SR endbulb (Lo1: CF, 1.0 kHz; SR, 0.01 s/s) as it contacts the soma of a spherical bushy cell. The HRP–DAB reaction product clearly distinguishes the labeled endings (arrows) from the unlabeled endings (arrowheads). The spherical bushy cell exhibits its characteristic accumulation of rough endoplasmic reticulum (ER) against one side of its nucleus, representing the Nissl cap (cap). Scale bar = 5 μm.

types of analyses were conducted because of the relatively large variability in vesicle counts due mostly to differences in the size and shape of ending profiles and by the presence or absence of PSDs in the profile. Individual profiles of high SR endbulbs (n = 122) had an average of 104.5 ± 93.9 synaptic vesicles, whereas those of low SR endbulbs (n = 127) had 82.9 ± 94.3. The conversion of these values to a standard unit of area (μm^2) produced a value of 67.2 ± 16.9 vesicles per μm^2 for high SR endings and 62.2 ± 24.4 vesicles per μm^2 for low SR endings. In either case, there are on average more synaptic vesicles in high SR endbulbs than in low SR endbulbs ($P < 0.05$). A summary of ending profile data including synaptic vesicle density, mitochondria size and number, and apposition lengths is shown in Table 2.

Synapses

Axosomatic and axodendritic synapses. The synapses of endbulbs have been described elsewhere (e.g., Lenn and Reese, 1966; Ibata and Pappas, 1976; Gulley et al., 1978; Cant and Morest, 1979; Ryugo and Sento, 1991). In addition to the well-known axosomatic synapses of endbulbs, there are also asymmetric, axodendritic synapses (Fig. 8A,C). On the side of the endbulb facing away from the spherical bushy cell somata, dendrites can be synaptically contacted. The dendritic profiles range in cross-sectional diameter from 2 to 10 μm and are distinguished in a single section from the grazing of a cell body by their lack of ribosomes and Golgi apparatus. We verified that they were dendrites by examining such profiles through a series of

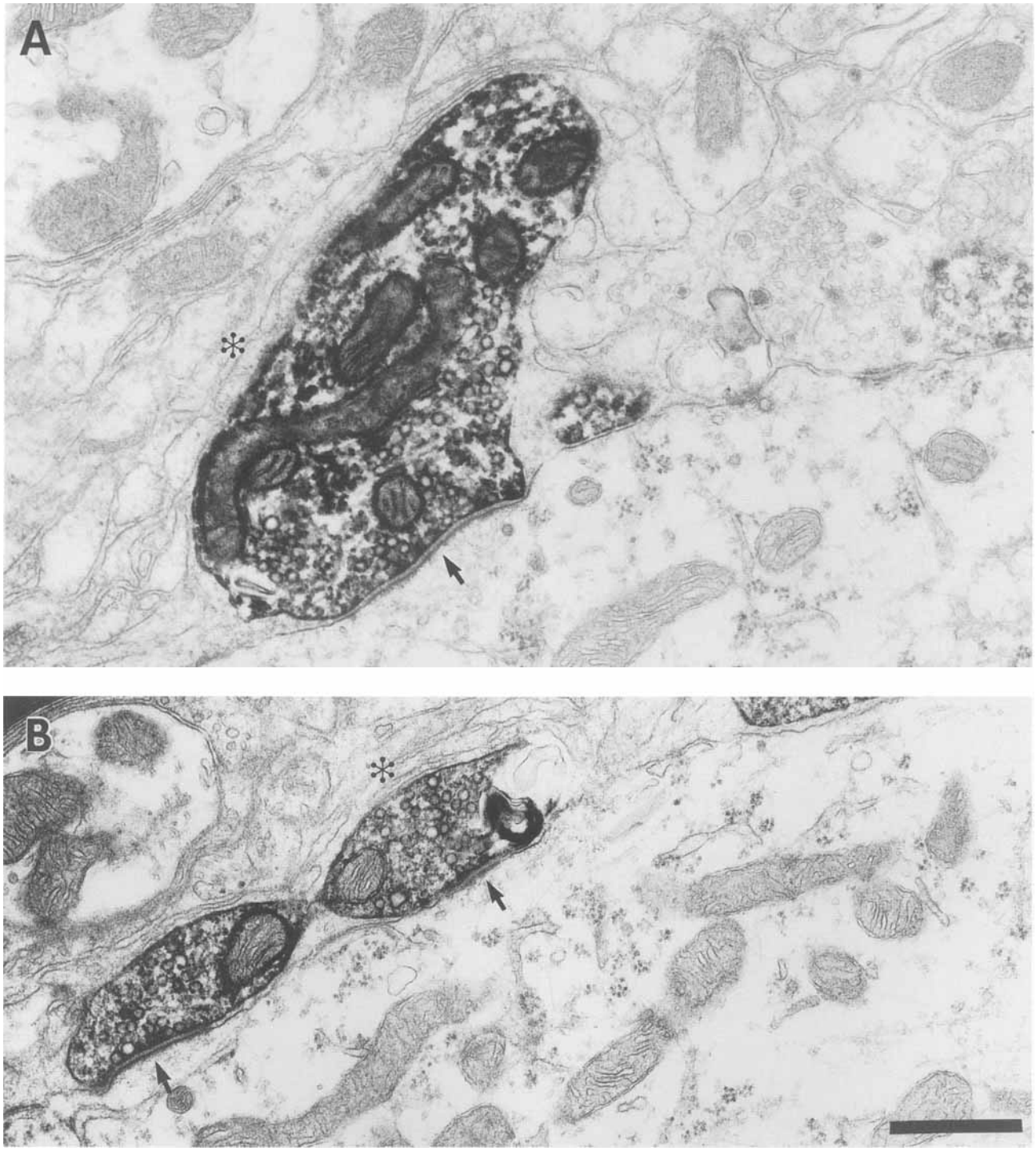

Fig. 6. **A–B:** Electron micrographs of labeled endings of low SR fibers. Note that the PSDs (arrows) are relatively long and exhibit little curvature. These micrographs also illustrate that ending profiles of low SR endbulbs are smaller and contain fewer synaptic vesicles than do those of high SR endbulbs (see Fig. 7). Glial processes (*) are closely applied to the endings. Scale bar = 0.5 μm.

many consecutive ultrathin sections. Endbulbs of the high SR fibers formed relatively more axodendritic synapses (13.6 ± 2.5% of a total of 878 PSDs) than did those of low SR fibers (2.9 ± 0.1% of a total of 622 PSDs).

Endbulbs of high and low SR fibers also differ in the manner by which they make axodendritic synapses. For high SR fibers, opposite poles of the endbulb surface form synapses: one side contacts the soma of a spherical bushy

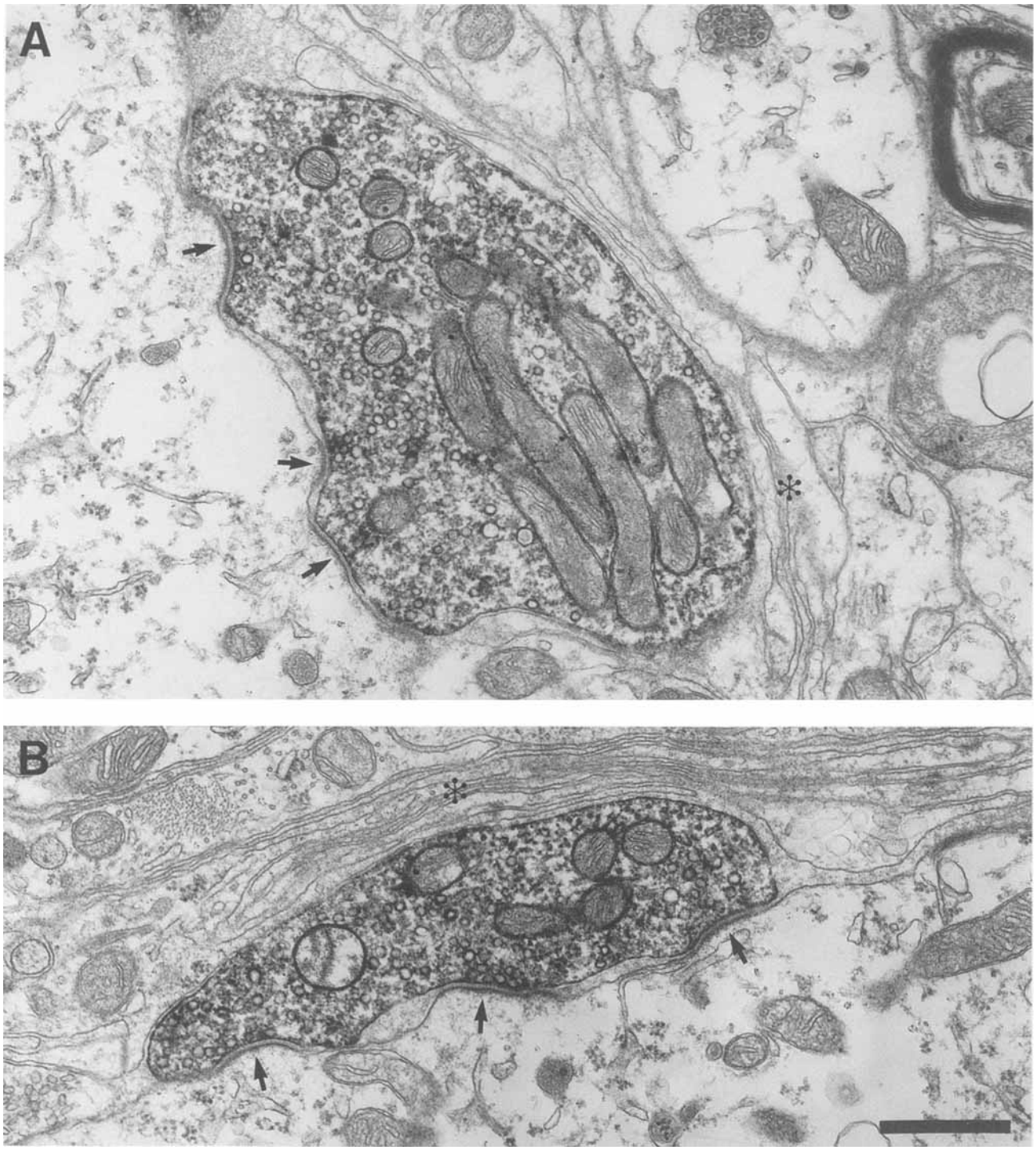

Fig. 7. **A–B:** Electron micrographs of labeled endings of high SR fibers. The PSDs are characteristically curved (arrows) and shorter than those endings of low SR fibers. These micrographs also illustrate that ending profiles of high SR fibers are larger than those of low SR fibers and have more synaptic vesicles (see Fig. 6). Glial processes (*) form multiple layers surrounding the primary endings. Scale bar = 0.5 μm.

cell, whereas the opposite side contacts dendrites in the immediately adjacent neuropil (Fig. 8C). In contrast, the endbulbs of low SR fibers made mostly axosomatic synapses. When axodendritic synapses were present, they tended to be made by short collaterals (Fig. 8B).

Curvature of postsynaptic densities. Postsynaptic densities exhibit three basic configurations: (1) straight, (2) concave, and (3) convex (Markus and Petit, 1989). A single endbulb will give rise to many synapses, and one striking feature of the postsynaptic density is its outward arch

TABLE 2. Summary of Ending Profiles (Mean ± S.D.)

	Profile size* (μm^2)	SVs/μm^2*	Mitochondria size* (μm^2)	Number of mitochondria (per profile)	Apposition length* (μm)
Low SR Endbulbs	1.63 ± 2.2	62.2 ± 24.4	0.061 ± 0.03	6.48 ± 6.0	1.72 ± 1.5
n[1]	151	127	151	151	127
High SR Endbulbs	2.04 ± 2.7	67.2 ± 16.9	0.070 ± 0.04	6.23 ± 7.3	2.03 ± 1.7
n[1]	158	122	158	158	122

[1]Number of profiles analyzed.
*$P < 0.05$ (Mann-Whitney U test) where statistical n is based on nine endbulbs.

toward the presynaptic ending. Typically, the endbulbs of both SR groups exhibited "convex" axosomatic densities (Figs. 6–8) and "straight" axodendritic densities (Fig. 8). The calculated curvature of axosomatic synapses (Cooke et al., 1974) revealed that, on average, PSDs of low SR endbulbs ($1/r = 1.80 \pm 2.5$, n = 575 PSDs) had a shallower arc than did those of high SR endbulbs ($1/r = 2.35 \pm 3.1$, n = 323 PSDs; $P < 0.003$).

The PSDs of axodendritic synapses were flatter than their axosomatic counterparts. There was, however, no difference in curvature when comparing PSDs of dendrites receiving endbulb synapses from high ($1/r = 0.27 \pm 1.8$, n = 42) versus low ($1/r = 0.24 \pm 0.7$, n = 19) SR fibers. The curvature of PSDs from the collaterals of low SR endbulbs was slightly greater ($1/r = 0.48 \pm 0.8$, n = 21).

Synapse size. We reconstructed a number of endbulb swellings through serial ultrathin sections. The alignment of adjacent PSDs and subsequent rotation using a computer-assisted three-dimensional reconstruction system revealed individual synapses as viewed en face (Fig. 9). The en face area of each synapse was measured because it indicated the magnitude of the active zone with the postsynaptic spherical bushy cell. A total of 65 synapses were reconstructed from the five endbulbs of low SR fibers, and they exhibited an average size of 0.179 ± 0.02 μm^2. In contrast, 74 synapses were reconstructed from the four endbulbs of high SR fibers, and these were, on average, significantly smaller (0.089 ± 0.02 μm^2). These differences in synapse size ($P < 0.01$) were maintained by endbulbs of the separate SR groupings and by each cat (Fig. 10).

Number of synapses per endbulb. The number of axosomatic synapses per endbulb was calculated in the following way. First, we counted the number of synapses per unit apposition area through serial section reconstructions of each endbulb. Although we determined only a few values for different regions of each endbulb, this value was fairly constant and indicated that synapse density was uniform over the entire endbulb. Consequently, we multiplied this value for each endbulb by its corresponding silhouette area, because the silhouette area should approximate the contact surface of the endbulb with the postsynaptic cell body. This method predicted that high SR endbulbs had an average of $1{,}720 \pm 395$ synapses and that low SR endbulbs had an average of 407 ± 139 synapses. These data indicate that high SR endbulbs have roughly four times the number of axosomatic synapses contacting spherical bushy cells as do low SR endbulbs. Furthermore, although the absolute values differed for each cat, the ratios were strikingly similar (Table 1).

On the basis of mean synapse size (Fig. 10, middle) and the calculated number of synapses per endbulb (Table 1), we estimated that high SR endbulbs have, on average, 156.9 ± 72.9 μm^2 total synaptic area contacting a spherical bushy cell body as opposed to 72.9 ± 25.9 μm^2 for low SR endbulbs. The absolute values were constant within cats and varied a bit across cats, but the relative values were consistent both within and across cats (Table 3).

DISCUSSION

In the present study, we examined endbulbs of Held from low and high SR auditory nerve fibers using intracellular HRP labeling techniques combined with light and electron microscopy. Endbulbs of Held are large axosomatic endings located in the anteroventral cochlear nucleus that arise from the myelinated axons of the auditory nerve (Held, 1893; Ramón y Cajal, 1909; Lorente de Nó, 1981; Ryugo and Fekete, 1982). These auditory nerve fibers have been systematically studied using anatomic and electrophysiologic methods, and they have been shown to exhibit dichotomous properties, including threshold at CF, dynamic range, maximum discharge rate (Kiang et al., 1965; Sachs and Abbas, 1974; Liberman, 1978; Kim and Molnar, 1979; Evans and Palmer, 1980), caliber of peripheral terminal and location of terminal under the inner hair cell (Liberman, 1982a), number, size, and distribution of central terminals (Fekete et al., 1984; Rouiller et al., 1986; Ryugo and Rouiller, 1988; Liberman, 1991), and appearance of endbulbs of Held (Sento and Ryugo, 1989; Ryugo and Sento, 1991). These differences are present across the entire range of CF values and imply that the different SR groups represent fundamentally distinct components for processing acoustic information. Furthermore, the data suggest that comparisons of the synaptic junctions between the separate SR fiber groups might provide new insights into structural specializations that accompany different levels of synaptic activity (Fig. 11).

Each auditory nerve fiber serves as a near one-to-one conduit from a single inner hair cell to a single spherical bushy cell. Thus, the mechanism by which signals are processed nerve to nucleus is hypothesized to be determined in large part by the nature of this primary synapse. Extracellular electrophysiologic recordings reveal that, in the anteroventral cochlear nucleus, the action potentials of the second order neuron are often preceded by the presence of small, positive potentials (Pfeiffer, 1966). These potentials are called "prepotentials" and always precede the action potentials by 0.5 ms. As a result, the prepotential is hypothesized to reflect the depolarization of the endbulb. The coupling of the prepotential to the postsynaptic spike reveals that the second-order primarylike unit faithfully follows the spike activity of the auditory nerve. Because the number of endbulbs per auditory nerve fiber is similar across the different SR groups (Fekete et al., 1984) and because endbulbs of different SR groups do not appear to converge on the same cell in the cochlear nucleus (Ryugo and Sento, 1991), the distribution of SR in the auditory nerve was expected to be the same as that of primarylike units in the AVCN (spherical bushy cells). Instead, there is

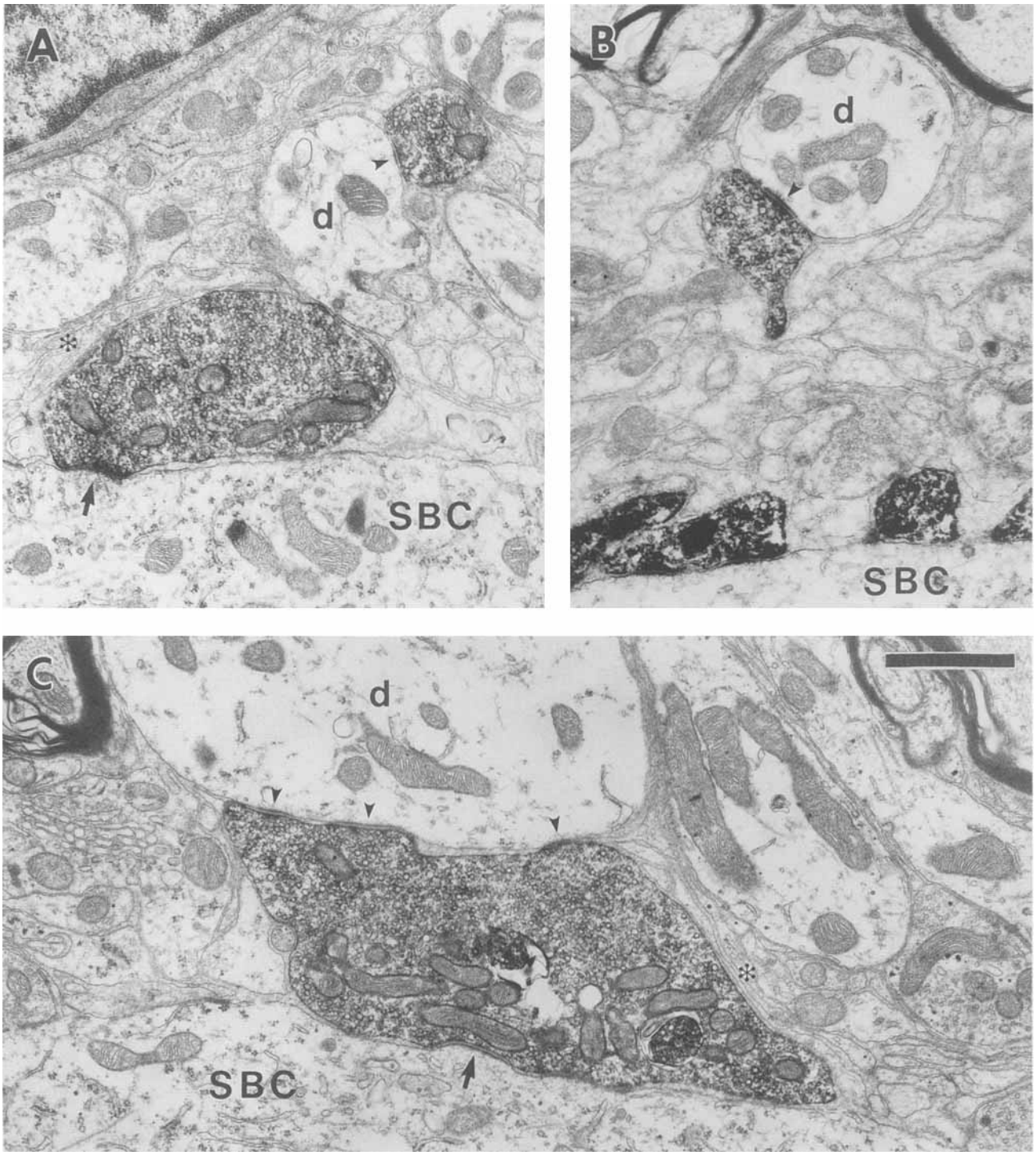

Fig. 8. Electron micrographs illustrate the appearance of axodendritic synapses formed by endbulbs of both SR groups. **A:** Example of an axodendritic synapse (arrowhead) formed by a labeled collateral of a low SR endbulb. The postsynaptic dendrite (d) is throught to arise from an adjacent spherical bushy cell (SBC). The main body of the endbulb forms an axosomatic synapse (arrow) with a spherical bushy cell. **B:** A labeled collateral from a different low SR endbulb forms an axodendritic synapse (arrowhead) with a thin dendritic profile (d). Labeled portions of the main body of the endbulb can be seen at the bottom of this micrograph. **C:** The main body of endbulbs of high SR fibers form axosomatic (arrow) and axodendritic (arrowheads) synapses as illustrated in this micrograph and form more of both types compared to endbulbs of low SR fibers. Glial processes (*) are also indicated. Scale bar = 1 μm.

an increase in high SR units from roughly 60% in the auditory nerve (Kiang et al., 1965; Liberman, 1978) to more than 85% in primarylike units with prepotentials the AVCN (Molnar and Pfeiffer, 1968). This altered distribution of SR from nerve to nucleus cannot be readily explained by the characteristics of axosomatic synapses of the endbulb.

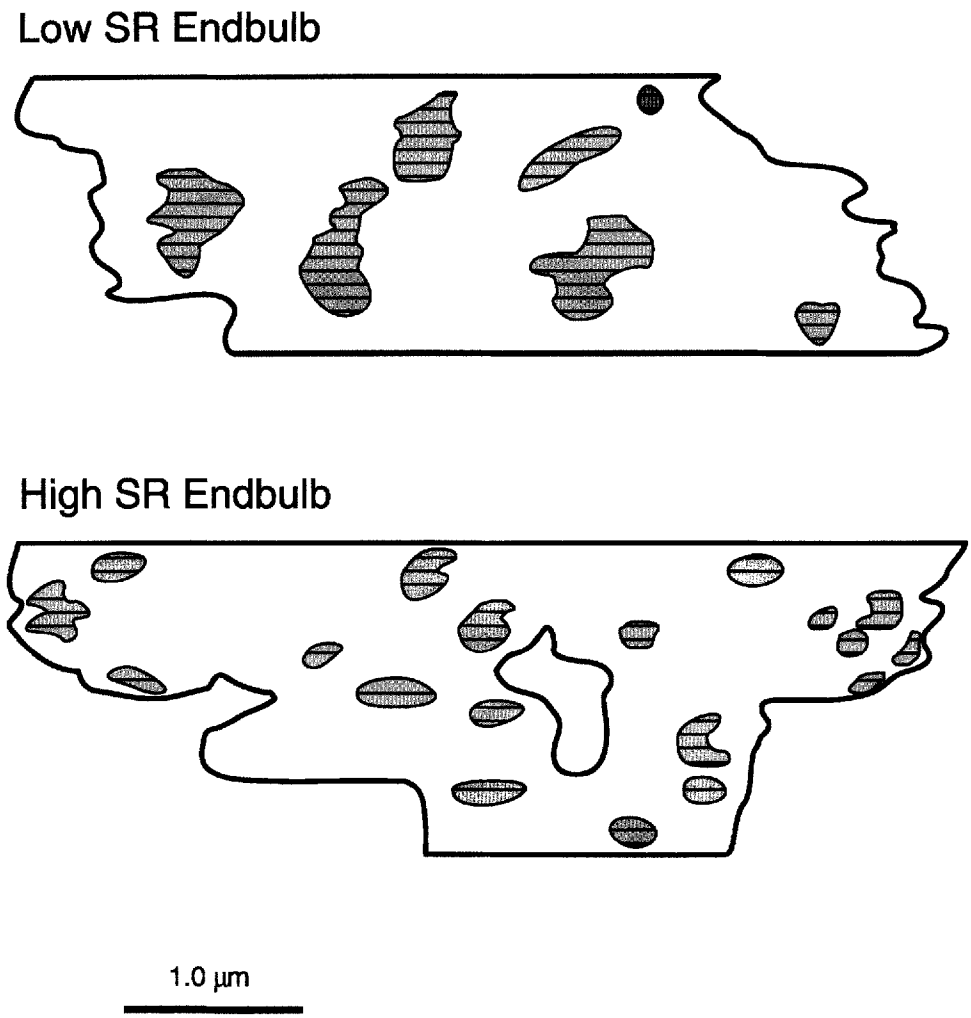

Fig. 9. The representative appearance of synaptic PSDs and apposition areas viewed *en face*. Labeled endings and synapses were reconstructed through serial ultrathin sections and then rotated using a computer-assisted system so that the ending apposition surface (bold outline) could be visualized. **Top:** Synapses from portion of low SR endbulb, Lo1. **Bottom:** Synapses from portion of high SR endbulb, Hi3. The reconstructed synapses are stippled and outlined. Each thin, parallel line represents a section. In general, low SR endbulbs have larger but fewer synapses than high SR endbulbs.

Endbulbs from both SR groups formed axosomatic and axodendritic synapses, but those from high SR fibers formed more axodendritic contacts than did those from low SR fibers. The way in which somata of spherical bushy cells are nestled in among the dendrites of other bushy cells and not their own suggests that these postsynaptic dendrites belong to nearby spherical bushy cells (Ryugo and Sento, 1991). One mechanism by which fibers of high SR activity might expand their influence in the AVCN is if axodendritic synapses from several endbulbs of high SR fibers are present on the dendrites of a spherical bushy cell that receives 1–2 endbulbs from low SR fibers. In this manner, axodendritic synapses would be responsible for transforming the SR distribution from auditory nerve to primarylike units in the cochlear nucleus.

Endbulb synapses, whether arising from high or low SR fibers, obviously provide faithful transmission of presynaptic activity to the postsynaptic neuron. Transmission at cochlear nerve synapses is thought to be mediated by an excitatory amino acid (Wenthold, 1985), specifically glutamate (Raman and Trussell, 1992; Zhou and Parks, 1992; Hunter et al., 1993; Zhang and Trussell, 1994). The rapid and highly efficient mechanisms for synaptic transmission may be facilitated by the presence of the glial lamellae that surround the synaptic endings. Historically, the glial processes were considered important components of synaptic glomeruli, which isolated synaptic elements from one another (Gray, 1961; Szentágothai, 1963; Peters and Palay, 1966). Glial processes, however, may also contain glutamate transporters (Storck et al., 1992; Mennerick and Zorumski, 1994; Rothstein et al., 1994) and play a role in keeping excess transmitter out of the synaptic cleft.

Synapse size

The synaptic active zone is represented in part by a flattened, irregularly shaped subcellular density that appears as a thickening of electron-dense material attached to the postsynaptic membrane when viewed in cross section. This postsynaptic thickening is a prominent specialization of the submembranous cytoplasm whose restricted localization within the membrane also implies a corresponding

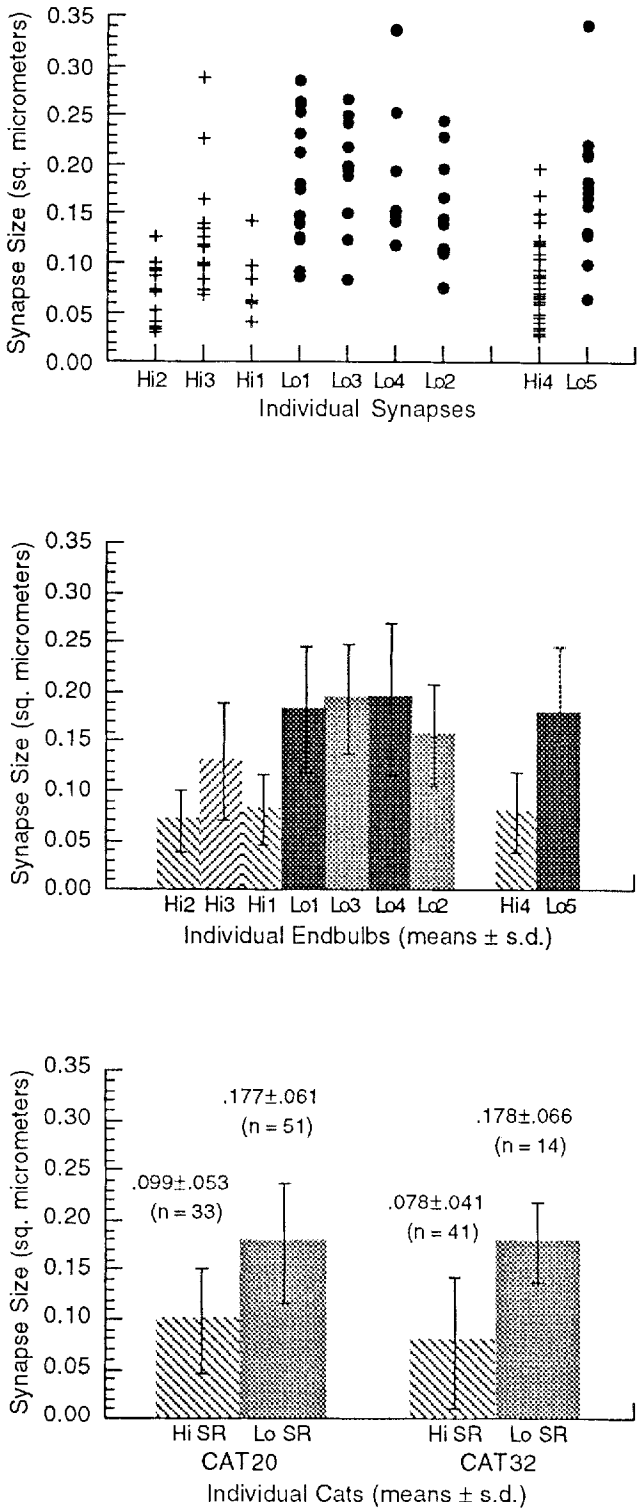

Fig. 10. Bar graphs illustrate individual synapse sizes (**top**), mean (±S.D.) synapse sizes for each endbulb (**middle**), and mean (±S.D.) synapse sizes for each cat (**bottom**). There is some overlap in individual synapse size among nerve fibers of different SRs, but size similarities within SR grouping and size differences across SR grouping are strikingly consistent.

TABLE 3. Summary of Synaptic Features (Mean ± S.D.)[1]

	PSD size[2] (μm^2)	PSD curvature[3] (1/radius)	Estimated total axosomatic synapses (per endbulb)	Axodendritic synapses[3] (% of somatic PSDs)
Low SR endbulbs (n = 5)	0.177 ± 0.06 (n = 65)	1.80 ± 2.5 (n = 575)	407 ± 139	2.9 ± 0.1 (n = 622)
High SR endbulbs (n = 4)	0.088 ± 0.05 (n = 74)	2.35 ± 3.1 (n = 323)	1,720 ± 395	13.6 ± 2.5 (n = 878)

[1]All comparisons between low versus high SR values have $P < 0.01$ (Mann-Whitney U test) where statistical n is based on nine endbulbs.
[2]n = Number of completely reconstructed synapses (or active zones).
[3]n = Number of postsynaptic densities analyzed.

specialization of the cytoskeletal matrix (Hirokawa, 1991). Apposed to this postsynaptic density is a presynaptic component that represents the rest of the synaptic active zone. The presynaptic component exhibits focal aggregations of dense material along the cytoplasmic surface of its membrane and an accumulation of synaptic vesicles. These specialized membrane appositions together with the synaptic cleft are also defined as the synapse, or synaptic complex.

The postsynaptic density contains the receptors for neurotransmitters (Seitanidou et al., 1988; Flucher and Daniels, 1989; Nusser et al., 1994) and is associated with Ca^{++}/calmodulin-dependent protein kinases (Kennedy, 1989). The postsynaptic membrane houses additional molecules involved in signal transduction including other receptors (e.g., metabotropic receptors), voltage-gated ion channels, and pumps. The presynaptic membrane is not only involved in vesicular release of transmitter for synaptic transmission (e.g., Katz, 1966) but also contains substrates involved in inactivating synaptic transmission such as re-uptake receptors and transporters. The number and spatial distribution of these molecules is hypothesized to determine synaptic mechanisms and modes of intercellular communication.

We demonstrated that the endbulbs of high SR fibers had smaller active zones than those of low SR fibers. Under normal conditions, high SR fibers have greater levels of spike activity than those of low SR fibers, implying that activity somehow causes a rearrangement of active zones into smaller but more numerous modules. This reorganization serves to bring more the nonactive zone membrane into closer proximity to the PSDs. The relative increase in PSD perimeter was speculated as being important for synaptic vesicle release (Peters and Kaiserman-Abramof, 1969) or perhaps synaptic vesicle turnover (Nieto-Sampetro et al., 1982), but these ideas remain to be verified. A different idea is that inactive fibers must compensate by ensuring that each action potential exerts maximal postsynaptic effects (Güldner and Ingram, 1980). One consequence might be an enlarged active zone with a (presumably) corresponding large number of transmitter receptors. This circumstance is manifest in low SR fibers of normal hearing cats and is greatly exaggerated by the enormous active zones found in spherical bushy cells of congenitally deaf cats (Huchton et al., 1995). Our data are certainly consistent with the notion that the PSD is a dynamic structure whose form is influenced by the activity of the synapse (Siekevitz, 1985; Rostas et al., 1992).

Active zones are surrounded by nonactive plasmalemma (e.g., Fig. 9). Nonactive zones undoubtedly contain other ion channels, receptors, and/or pumps. For example, metabotropic glutamate receptors (cerebellar cortex: Baude et al.,

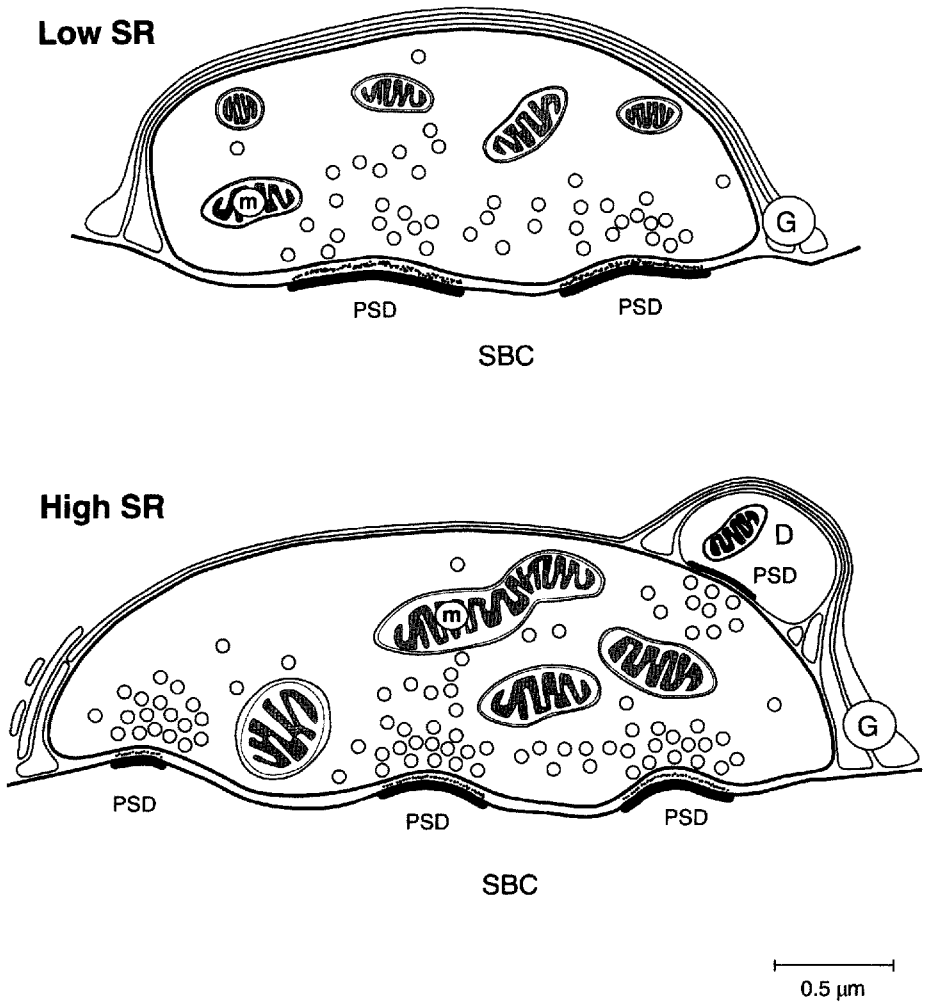

Fig. 11. Schematic drawing highlights the structural features typical of each ending class with respect to fiber SR. Both endings are ensheathed by glial processes. The ending of low SR fibers express larger but fewer synapses, exhibit less curvature of their postsynaptic densities, contain fewer synaptic vesicles, and have smaller mitochondria. In contrast, endings of high SR fibers express smaller but more numerous synapses, exhibit greater curvature of their postsynaptic densities, contain more synaptic vesicles, have larger mitochondria, and form more axodendritic synapses. D, dendrite; G, glial processes; m, mitochondria; PSD, postsynaptic density; SBC, spherical bushy cell.

1993; Nusser et al., 1994) and Na^+ channels (neuromuscular junction: Flucher and Daniels, 1989) are concentrated in the membrane surrounding PSDs. A pattern of multiple, small active zones may be more advantageous than a single large active zone for facilitating movement of ions, metabolites, and/or molecules from PSD to non-PSD regions. On the presynaptic side, this pattern of multiple, small synapses would also allow for vesicle attachment sites and recycling of synaptic vesicles to be in closer proximity to each active zone. This arrangement could serve to keep transporters and/or reuptake receptors near the transmitter release sites, thereby providing greater efficiency. Rapid removal of excess transmitter in the cleft would reduce desensitization of receptors at the synapse (Trussell and Fischbach, 1989).

By inference, both pre- and postsynaptic specializations must orchestrate their own unique spatial assemblage when forming synaptic junctions. In the AVCN, it seems that signals, as yet unidentified, would be exchanged in both directions between the endbulbs and spherical bushy cells to accomplish this task. The apparent interactive construction of pre- and postsynaptic components of the active zone is evident not only in the case of excitatory and inhibitory synapses (e.g., Gray, 1959) but also in our observations of activity-related synaptic structure.

Synaptic rearrangement

Variations in active zone size and shape have been demonstrated after manipulations of both auditory (Rees et al., 1985) and visual (Vrensen and Cardozo, 1981; Güldner and Phillips, 1985; Bakkum et al., 1991) systems. These studies reported that decreased neural activity caused by sensory deprivation produced larger synaptic areas when compared with normal controls. One explanation for this plasticity is that activity-induced increases of Ca^{++} levels in the postsynaptic cell induces some enzyme to shrink the PSD (Rees et al., 1985; Melloni and Pontremoli, 1989).

A different role for enzymatic degradation of the PSD in response to increased activity was thought to underlie a

mechanism for synaptic division and the formation of new synapses (Carlin and Siekevitz, 1983; Dyson and Jones, 1984). It was hypothesized that high levels of neural stimulation resulted in the formation of a "synaptic spinule," which is an evagination of membrane and cytoplasm within the PSD material. This spinule was proposed as a site of membrane recycling resulting from the turnover of synaptic vesicle membranes during periods of high neurotransmitter release. The presence of this spinule possibly provided membrane for reorganizing the PSD so that irregularly shaped synapses could be formed. This new population of synapses could represent a more permanent expression of enhanced contact and synaptic transmission, where the irregularities represent smaller component synapses that might be more effective than a single, large synapse (Edwards, 1995).

Synaptic curvature

The curvature of PSDs also differs between synapses of high versus low activity terminals (Pysh, 1972; Devon and Jones, 1981; Wesa et al., 1982; Dickinson-Nelson and Reese, 1983; Van Huizen et al., 1987; Bakkum et al., 1991). This feature could be indicative of the merging of synaptic vesicle membrane with plasma membrane at the synapse. The synaptic junction between endbulbs and spherical bushy cells has been described as a "dome-shaped evagination of the postsynaptic membrane" using freeze fracture and transmission electron microscopic techniques (Gulley et al., 1978). When viewed in transmission electron micrographs, PSDs of endbulbs have a typical convex curvature of postsynaptic density into the presynaptic membrane, and we have shown that high SR endbulbs exhibit greater curvature than do low SR endbulbs. Such a configuration could result from prolonged differences in synaptic activity.

Synaptic vesicles

Because vesicle turnover may be an important factor affecting PSD morphology, we studied the population of vesicles in endbulbs of different SR fibers. There is considerable variability in, yet a distinct separation of, the SR groups in that low SR endbulbs exhibited fewer vesicles per arbitrary unit (e.g., μm^2 or PSD) than did high SR endbulbs. The rapidity of synaptic vesicle fusion and turnover possibly contributes somewhat to the variability in vesicle density for any particular ending, but our data nonetheless suggest that active endings contain more vesicles. Presumably, this feature reflects the necessary preparation of the ending for continuous release of vesicles in response to activity. Studies that have examined synapses after depletion of vesicles have shown that a subpopulation of vesicles remains in the synapse, which may not be directly involved in synaptic transmission (Koenig et al., 1989). In this context, we found that synaptic vesicles differed in size with regard to their proximity to PSDs. This small but reliable size difference may reflect the known difference in synaptic vesicle pools, where the smaller vesicles reflect a reserve pool and the larger vesicles represent the releasable pool.

Summary

Endbulbs form part of the complex organization of synapses in the cochlear nucleus and express many structural features necessary for efficient transmission of information from one cell to the next. They are large and encased in glial lamellae. The endbulbs of high SR auditory nerve fibers contain roughly four times as many synapses as do the endbulbs of low SR fibers and twice the total active zone area. Individual active zones of high SR endbulbs are hypothesized to have facilitated access to peripheral ion channels, pumps, and other receptors when compared with those of low SR fibers by virtue of their smaller size. High SR endbulbs exhibit other morphologic features that also emphasize high activity levels, including increased synaptic vesicle density, mitochondrial number, and PSD curvature. These data are consistent with the idea that synaptic endings are highly specialized and morphologically plastic structures whose form may reflect the physiologic demands from moment to moment.

ACKNOWLEDGMENTS

We gratefully thank Rachael Urik for technical assistance and John R. Doucet, David M. Huchton, Ahmed A. Saada, Diana L. Weedman, and Debora D. Wright for helpful discussions of the data and critical reading of the manuscript. This work was supported by NIH grant DC00232. M.M.W. was supported by NIH training grant DC00027.

LITERATURE CITED

Bakin, J.S., and N.M. Weinberger (1990) Classical conditioning induces CS-specific receptive field plasticity in the auditory cortex of the guinea pig. Brain Res. *536:*271–286.

Bakkum, B.W., L.A. Benevento, and R.S. Cohen (1991) Effects of light/dark- and dark-rearing on synaptic morphology in the superior colliculus and visual cortex of the postnatal and adult rat. J. Neurosci. Res. *28:*65–80.

Baude, A., Z. Nusser, J.D.B. Roberts, E. Mulvihill, R.A.J. McIlhinney, and P. Somogyi (1993) The metabotropic glutamate receptor (mGluR1α) is concentrated at perisynaptic membrane of neuronal subpopulations as detected by immunogold reaction. Neuron *11:*771–787.

Benson, T.W., D.K. Ryugo, and J.W. Hinds (1984) Effects of sensory deprivation on the developing mouse olfactory system: A light and electron microscopic, morphometric analysis. J. Neurosci. *4:*638–653.

Born, D.E., and E.W. Rubel (1985) Afferent influences on brain stem auditory nuclei of the chicken: Neuron number and size following cochlea removal. J. Comp. Neurol. *231:*435–445.

Born, D.E., D. Durham, and E.W. Rubel (1991) Afferent influences on brainstem auditory nuclei of the chick: Nucleus magnocellularis neuronal activity following cochlea removal. Brain Res. *557:*37–47.

Bourk, T.R., J.P. Mielcarz, and B.E. Norris (1981) Tonotopic organization of the anteroventral cochlear nucleus of the cat. Hear. Res. *4:*215–241.

Boyne, A.F., T.P. Bohan, and T.H. Williams (1975) Changes in cholinergic synaptic vesicle populations and the ultrastructure of the nerve terminal membranes of *Narcine brasiliensis* electric organ stimulated to fatigue *in vivo*. J. Cell Biol. *67:*814–825.

Burwen, S.J., and B.H. Satir (1977) Plasma membrane folds on the mast cell surface and their relationship to secretory activity. J. Cell Biol. *74:*690–697.

Cant, N.B., and D.K. Morest (1979) Bushy cells in the anteroventral cochlear nucleus of the cat: A study with the electron microscope. Neuroscience *4:*1925–1945.

Carlin, R.K., and P. Siekevitz (1983) Plasticity in the nervous system: Do synapses divide? Proc. Natl. Acad. Sci. USA *80:*3517–3521.

Cooke, C.K., T.M. Nolan, S.E. Dyson, and D.G. Jones (1974) Pentobarbital-induced configurational changes at the synapse. Brain Res. *76:*330–335.

Devon, R.M., and D.G. Jones (1981) Synaptic parameters in developing rat cerebral cortex: Comparison of anaesthetized and unanaesthetized states. Dev. Neurosci. *4:*351–362.

Diamond, M.E., M. Armstrong-James, and F.F. Ebner (1993) Experience-dependent plasticity in adult rat barrel cortex. Proc. Natl. Acad. Sci. USA *90:*2082–2086.

Dickinson-Nelson, A., and T.S. Reese (1983) Structural changes during transmitter release at synapses in the frog sympathetic ganglion. J. Neurosci. *3:*42–52.

Dyson, S.E., and D.G. Jones (1984) Synaptic remodelling during development and maturation: Junction differentiation and splitting as a mechanism for modifying connectivity. Dev. Brain Res. *13:*125–137.

Edwards, F.A. (1995) LTP—A structural model to explain the inconsistencies. Trends Neurosci. *18:*250–255.

Evans, E.F., and A.R. Palmer (1980) Relationship between the dynamic range of cochlear nerve fibers and their spontaneous activity. Exp. Brain Res. *40:*115–118.

Fekete, D.M., E.M. Rouiller, M.C. Liberman, and D.K. Ryugo (1984) The central projections of intracellularly labeled auditory nerve fibers in cats. J. Comp. Neurol. *229:*432–450.

Fifková, E., and M. Morales (1992) Actin matrix of dendritic spines, synaptic plasticity, and long-term potentiation. Int. Rev. Cytol. *139:*267–307.

Fifková, E., and A. van Harreveld (1977) Long-lasting morphological changes in dendritic spines of dentate granular cells following stimulation of the entorhinal area. J. Neurocytol. *6:*211–230.

Flucher, B.E., and M.P. Daniels (1989) Distribution of Na+ channels and ankyrin in neuromuscular junctions is complementary to that of acetylcholine receptors and the 43 KD protein. Neuron *3:*163–175.

Gil-Loyzaga, P., and R. Pujol (1990) Neurotoxicity of kainic acid in the rat cochlea during early developmental stages. Eur. Arch. Otorhinolaryngol. *248:*40–48.

Gilbert, C.D., and T.N. Wiesel (1990) Receptive field dynamics in adult primary visual cortex. Nature *356:*150–152.

Goodman, C.S., and C.J. Shatz (1993) Developmental mechanisms that generate precise patterns of neuronal connectivity. Neuron *72(10):*77–98.

Gray, E. (1959) Axo-somatic and axo-dendritic synapses of the cerebral cortex: An electron microscopic study. J. Anat. (Lond.) *93:*420–433.

Gray, E. (1961) The granule cells, mossy synapses and Purkinje spine synapses of the cerebellum: Light and electron microscopic observations. J. Anat. (Lond.) *95:*345–356.

Güldner, F.-H., and C.A. Ingram (1980) Increase in postsynaptic density material in optic target neurons of the rat suprachiasmatic nucleus after bilateral enucleation. Neurosci. Lett. *17:*27–31.

Güldner, F.-H., and S.C. Phillips (1985) Structural plasticity of developing optic synapses under different lighting conditions. Neurosci. Lett. *55:*225–228.

Gulley, R.L., D.M.D. Landis, and T.S. Reese (1978) Internal organization of membranes at end bulbs of Held in the anteroventral cochlear nucleus. J. Comp. Neurol. *180:*707–742.

Hashisaki, G.T., and E.W. Rubel (1989) Effects of unilateral cochlea removal on anteroventral cochlear nucleus neurons in developing gerbil. J. Comp. Neurol. *283:*465–473.

Held, H. (1893) Die centrale Gehorleitung. Arch. Anat. Physiol. Anat. Abt. 201–248.

Heuser, J.E., and T.S. Reese (1973) Evidence for recycling of synaptic vesicle membrane during transmitter release at the frog neuromuscular junction. J. Cell Biol. *57:*315–344.

Hirokawa, N. (1991) Molecular architecture and dynamics of the neuronal cytoskeleton. In R.D. Burgoyne (ed): The Neuronal Cytoskeleton. New York: Wiley-Liss, pp. 5–74.

Huchton, D.M., T. Pongstaporn, J.K. Niparko, and D.K. Ryugo (1995) Ultrastructural features of endbulbs of Held in deaf white cats: Changes in structure related to age of deafness. Otol. Head Neck Surg., Abstr, *113:*100.

Hunter, C., R.S. Petralia, T. Vu, and R.J. Wenthold (1993) Expression of AMPA-selective glutamate receptor subunits in morphologically defined neurons of the mammalian cochlear nucleus. J. Neurosci. *13:*1932–1946.

Ibata, Y., and G.D. Pappas (1976) The fine structure of synapses in relation to the large spherical neurons in the anterior ventral cochlear (sic) of the cat. J. Neurocytol. *5:*395–406.

Kaas, J.H. (1991) Plasticity of sensory and motor maps in adult mammals. Ann. Rev. Neurosci. *14:*137–167.

Katz, B. (1966) Nerve, Muscle, and Synapse, New York: McGraw-Hill.

Kennedy, M.B. (1989) Regulation of neuronal function by calcium. Trends Neurosci. *12:*417–420.

Kiang, N.Y.-S., T. Watanabe, E.C. Thomas, and L.F. Clark (1965) Discharge Patterns of Single Fibers in the Cat's Auditory Nerve. Cambridge: MIT Press.

Kiang, N.Y.-S., J.M. Rho, C.C. Northrop, M.C. Liberman, D.K. Ryugo (1982) Hair-cell innervation by spiral ganglion cells in adult cats. Science *217(4555):*175–177.

Kim, D.O., and C.E. Molnar (1979) A population study of cochlear nerve fibres: Comparison of spatial distributions of average rate and phase-locking measures of responses to single tones. J. Neurophysiol. *42:*16–30.

Koenig, J.H., T. Kosaka, and K. Ikeda (1989) The relationship between the number of synaptic vesicles and the amount of transmitter released. J. Neurosci. *9(6):*1937–1942.

Leake, P.A., and G.T. Hradek (1988) Cochlear pathology of long term neomycin induced deafness in cats. Hear. Res. *33:*11–34.

Lenn, N.Y., and T.S. Reese (1966) The fine structure of nerve endings in the nucleus of the trapezoid body and the ventral cochlear nucleus. Am. J. Anat. *118:*375–389.

LeVay, S., T.N. Wiesel, and D.H. Hubel (1980) The development of ocular dominance columns in normal and visually deprived monkeys. J. Comp. Neurol. *191:*1–51.

Liberman, M.C. (1978) Auditory-nerve responses from cats raised in a low-noise chamber. J. Acoust. Soc. Am. *63:*442–455.

Liberman, M.C. (1982a) Single-neuron labeling in the cat auditory nerve. Science *216:*1239–1241.

Liberman, M.C. (1982b) The cochlear frequency map for the cat: Labeling auditory-nerve fibers of known characteristic frequency. J. Acoust. Soc. Am. *72:*1441–1449.

Liberman, M.C. (1991) Central projections of auditory-nerve fibers of differing spontaneous rate. I. Anteroventral cochlear nucleus. J. Comp. Neurol. *313:*240–258.

Lorente de Nó, R. (1981) The Primary Acoustic Nuclei. New York: Raven Press.

Markus, E.J., and T.L. Petit (1989) Synaptic structural plasticity: Role of synaptic shape. Synapse *3:*1–11.

Melloni, E., and S. Pontremoli (1989) The calpains. Trends Neurosci. *12:*438–443.

Mennerick, S., and C.F. Zorumski (1994) Glial contributions to excitatory neurotransmission in cultured hippocampal cells. Nature *368:*59–62.

Molnar, C.E., and R.R. Pfeiffer (1968) Interpretation of spontaneous spike discharge patterns of neurons in the cochlear nucleus. Proceed. IEEE *56:*993–1004.

Moore, D.R. (1985) Postnatal development of the mammalian central auditory system and the neural consequences of auditory deprivation. Acta Otolaryngol. (Stochk) *421*(Suppl.):19–30.

Moore, D.R., and N.E. Kowalchuk (1988) Auditory brainstem of the ferret: Effects of unilateral cochlear lesions on cochlear nucleus volume and projections to the inferior colliculus. J. Comp. Neurol. *272:*503–515.

Nieto-Sampetro, M., S.F. Hoff, and C.W. Cotman (1982) Perforated postsynaptic densities: Probably intermediates in the synapse turnover. Proc. Natl. Acad. Sci. USA *79:*7518–7522.

Nordeen, K.W., H.P. Killackey, and L.M. Kitzes (1983) Ascending projections to the inferior colliculus following unilateral cochlear ablation in the neonatal gerbil, *Meriones unguiculatus.* J. Comp. Neurol. *214:*144–153.

Nusser, Z., E. Mulvihill, P. Streit, and P. Somogyi (1994) Subsynaptic segregation of metabotropic and ionotropic glutamate receptors as revealed by immunogold localization. Neuroscience *61:*421–427.

Osen, K.K. (1969) Cytoarchitecture of the cochlear nuclei in the cat. J. Comp. Neurol. *136:*453–484.

Parks, T.N. (1979) Afferent influences on the development of the brain stem auditory nuclei of the chicken: Otocyst ablation. J. Comp. Neurol. *183:*665–678.

Pasik, T.R., D.R. Moore, and E.W. Rubel (1994) Effect of altered neuronal activity on cell size in the medial nucleus of the trapezoid body and ventral cochlear nucleus of the gerbil. J. Comp. Neurol. *348:*111–120.

Peters, A., and I.R. Kaiserman-Abramof (1969) The small pyramidal neuron of the rat cerebral cortex. The synapses upon dendritic spines. Z. Zellforsch. Mikorsk. Anat. *100:*487–506.

Peters, A., and S.L. Palay (1966) The morphology of laminae A and A_1 of the dorsal nucleus of the lateral geniculate body of the cat. J. Anat. (Lond.) *100:*451–486.

Pfeiffer, R.R. (1966) Anteroventral cochlear nucleus: Wave forms of extracellularly recorded spike potentials. Science *154:*667–668.

Powell, T.P.S., and S.D. Erulkar (1962) Transneuronal cell degeneration in the auditory relay nuclei of the cat. J. Anat. (Lond.) *96:*249–268.

Pysh, J.J. (1972) Morphological alterations of synapses in electrically stimulated superior cervical ganglia of the cat. Science *176:*191–193.

Raman, I.M., and L.O. Trussell (1992) The kinetics of the response to glutamate and kainate in neurons of the avian cochlear nucleus. Neuron *9:*173–186.

Ramón y Cajal, S. (1909) Histologie du Système Nerveux de l'Homme et des Vertébrés, vol. I. Madrid: Instituto Ramón y Cajal (1952 reprint).

Recanzone, G.H., C.E. Schreiner, and M.M. Merzenich (1993) Plasticity in the frequency representation of primary auditory cortex following discrimination training in adult owl monkeys. J. Neurosci. *13:*87–103.

Rees, S., F.-H. Güldner, and L. Aitkin (1985) Activity dependent plasticity of postsynaptic density structure in the ventral cochlear nucleus of the rat. Brain Res. *325:*370–374.

Robertson, D., and D.R. Irvine (1989) Plasticity of frequency organization in auditory cortex of guinea pigs with partial unilateral deafness. J. Comp. Neurol. *282:*456–471.

Rostas, J.A.P., J.M. Kavanaugh, P.R. Dodd, J.W. Heath, and D.A. Powis (1992) Mechanisms of synaptic plasticity: Changes in postsynaptic densities and glutamate receptors in chicken forebrain during maturation. Mol. Neurobiol. *5(2–4):*203–216.

Rothstein, J.D., L. Martin, A.I. Levey, M. Dykes-Hoberg, L. Jin, D. Wu, N. Nash, and R.W. Kuncl (1994) Localization of neuronal and glial glutamate transporters. Neuron *13:*713–725.

Rouiller, E.M., R. Cronin-Schreiber, D.M. Fekete, and D.K. Ryugo (1986) The central projections of intracellularly labeled auditory nerve fibers: An analysis of terminal morphology. J. Comp. Neurol. *249:*261–278.

Ryugo, D.K. (1992) The auditory nerve: Peripheral innervation, cell body morphology, and central projections. In D.B. Webster (ed): Mammalian Auditory Pathway: Neuroanatomy. New York: Springer-Verlag, pp. 23–65.

Ryugo, D.K., and D.M. Fekete (1982) Morphology of primary axosomatic endings in the anteroventral cochlear nucleus of the cat: A study of the endbulbs of Held. J. Comp. Neurol. *210:*239–257.

Ryugo, D.K., and S.K. May (1993) The projections of intracellularly labeled auditory nerve fibers to the dorsal cochlear nucleus of cats. J. Comp. Neurol. *329:*20–35.

Ryugo, D.K., and E.M. Rouiller (1988) The central projections of intracellularly labeled auditory nerve fibers in cats: Morphometric correlations with physiological properties. J. Comp. Neurol. *271:*130–142.

Ryugo, D.K., and S. Sento (1991) Synaptic connections of the auditory nerve in cats: Relationship between endbulbs of Held and spherical bushy cells. J. Comp. Neurol. *305:*35–48.

Sachs, M.B., and P.J. Abbas (1974) Rate versus level functions for auditory-nerve fibers in cats: Tone-burst stimulation. J. Acoust. Soc. Am. *56:*1835–1847.

Schwaber, M.K., P.E. Garraghty, and J.H. Kaas (1993) Neuroplasticity of the adult primary auditory cortex following cochlear hearing loss. Am. J. Otol. *14:*252–258.

Seitanidou, T., A. Triller, and H. Korn (1988) Distribution of glycine receptors on the membrane of a central neuron: An immunoelectron microscopy study. J. Neurosci. *8:*4319–4333.

Sento, S., and D.K. Ryugo (1989) Endbulbs of Held and spherical bushy cells in cats: Morphological correlates with physiological properties. J. Comp. Neurol. *280:*553–562.

Shatz, C.J. (1990) Impulse activity and the patterning of connections during CNS development. Neuron *5:*745–756.

Shatz, C.J., and M.P. Stryker (1978) Ocular dominance in layer IV of the cat's visual cortex and the effects of monocular deprivation. J. Physiol. *281:*267–283.

Shatz, C.J., and M.P. Stryker (1988) Prenatal tetrodotoxin infusion blocks segregation of retinogeniculate afferents. Science *242:*87–89.

Sie, K.C.Y., and E.W. Rubel (1992) Rapid changes in protein synthesis and cell size in the cochlear nucleus following eighth nerve activity blockade or cochlea ablation. J. Comp. Neurol. *320:*501–508.

Siekevitz, P. (1985) The postsynaptic density: A possible role in the long-lasting effects in the central nervous system. Proc. Natl. Acad. Sci. USA *82:*3494–3498.

Sokolich, W.G. (1977) Improved acoustic system for auditory research. J. Acoust. Soc. Am. *62*(Suppl.):512.

Spoendlin, H. (1978) The afferent innervation of the cochlea. In R.F. Naunton and C. Fernandez (eds): Evoked Electrical Activity in the Auditory Nervous System. New York: Academic Press, pp. 21–41.

Storck, T., S. Schulte, K. Hofmann, and W. Stoffel (1992) Structure, expression, and functional analysis of a Na(+)-dependent glutamate/aspartate transporter from rat brain. Proc. Natl. Acad. Sci. USA *89:*10955–10959.

Szentágothai, J. (1963) The structure of the synapse in the lateral geniculate body. Acta Anat. *55:*166–185.

Trune, D.R. (1982) Influence of neonatal cochlear removal on the development of mouse cochlear nucleus: I. Number, size, and density of its neurons. J. Comp. Neurol. *209:*409–424.

Trussell, L.O., and G.D. Fischbach (1989) Glutamate receptor desensitization and its role in synaptic transmission. Neuron *3:*209–218.

Tucci, D.L., D.E. Born, and E.W. Rubel (1987) Changes in spontaneous activity and CNS morphology associated with conductive and sensorineural hearing loss in chickens. Ann. Otol. Rhinol. Laryngol. *96:*343–350.

Van der Loos, H., and T.A. Woolsey (1973) Somatosensory cortex: Structural alterations following early injury to sense organs. Science *179:*395–398.

Van Huizen, F., H.J. Romijn, and M.A. Corner (1987) Indications for a critical period for synapse elimination in developing rat cerebral cortex cultures. Brain Res. *428:*1–6.

Vrensen, G., and J.N. Cardozo (1981) Changes in size and shape of synaptic connections after visual training: An ultrastructural approach of synaptic plasticity. Brain Res. *218:*79–97.

Weinberger, N.M. (1995) Dynamic regulation of receptive fields and maps in the adult sensory cortex. Ann. Rev. Neurosci. *18:*129–158.

Weinberger, N.M., R. Javid, and B. Lepan (1993) Long-term retention of learning-induced receptive-field plasticity in the auditory cortex. Proc. Natl. Acad. Sci. USA *90:*2394–2398.

Weisel, T.N., and D.H. Hubel (1963) Effects of visual deprivation on morphology and physiology of cells in the cat's lateral geniculate body. J. Neurophysiol. *26:*973–993.

Wenthold, R.J. (1985) Glutamate and aspartate as neurotransmitters of the auditory nerve. In D.G. Drescher (ed): Auditory Biochemistry. Springfield: Thomas, pp. 125–140.

Wesa, J.M., F.-L.F. Chang, W.T. Greenough, and R.W. West (1982) Synaptic contact curvature: Effects of differential rearing on rat occipital cortex. Dev. Brain Res. *4:*253–257.

Zhang, S., and L.O. Trussell (1994) A characterization of excitatory postsynaptic potentials in the avian nucleus magnocellularis. J. Neurophysiol. *72:*705–718.

Zhou, N., and T.N. Parks (1992) γ-D-glutamylaminomethyl sulfonic acid (GAMS) distinguishes subtypes of glutamate receptor in the chick cochlear nucleus (nuc. magnocellularis). Hear. Res. *60:*20–26.